International Journal of Mass Spectrometry 294 (2010) 40–46

Contents lists available at ScienceDirect

International Journal of Mass Spectrometry

journal homepage: www.elsevier.com/locate/ijms

Dissociation of the phenylphosphine molecular ion: A theoretical study

Sun Young Kim, Joong Chul Choe*

Department of Chemistry, Dongguk University-Seoul, Seoul 100-715, Republic of Korea

ARTICLE INFO

Article history:
Received 7 April 2010
Received in revised form 3 May 2010
Accepted 3 May 2010
Available online 10 May 2010

Keywords:
Potential energy surface
DFT calculation
RRKM calculation
Kinetic
Reaction pathway

ABSTRACT

The potential energy surfaces (PESs) for the primary and secondary dissociations of the phenylphosphine molecular ion (**1a**) were determined from the quantum chemical calculations using the G3//B3LYP method. Based on the PESs, Rice–Ramsperger–Kassel–Marcus model calculations were performed for the individual unimolecular reaction steps in order to investigate the overall dissociation kinetics. At low internal energies of **1a**, the predominant dissociation channel was the formation of the phenylphosphinidene radical cation (**3a**) by the loss of H_2. At high energies, the formation of the phenylphosphenium ion (**2a**) by the loss of H• competed with the loss of H_2. The $C_6H_4P^+$ ion was mainly formed by the further dissociation of **3a** to the benzophosphirenium ion and H•. The reaction pathways for the formation of the major products in the secondary dissociation of **2a** were examined. The seven-membered ring isomer of **2a**, 7-phospha-tropylium ion, was hardly formed in the primary dissociation but played a role as an intermediate in the loss of C_2H_2 or HCP from **2a**. In this study, the kinetics analysis agreed well with previous experimental results.

1. Introduction

Ionized monosubstituted benzenes are among the most extensively studied compounds in gas phase ion chemistry. Especially, the dissociation of the molecular ions of $C_6H_5XH_n$, such as toluene (X = C) [1–4], aniline (X = N) [5–8], phenylsilane (X = Si) [9–11], and phenylphosphine (X = P) [12–14], has been investigated using various experimental and theoretical methods. The kinetics and mechanisms of some of the competitive and/or consecutive dissociations have been well understood. Interestingly, ring expansion, contraction, or opening can play an important role in the dissociation mechanisms of the molecular ions.

The $C_7H_7^+$ peak is the most abundant in the 70-eV electron ionization (EI) mass spectrum of toluene [15]. The loss of H• from the toluene molecular ion produces a mixture of benzylium and tropylium ions, at ratios that depend on the ion internal energy [2]. In contrast, in the EI mass spectrum of phenylsilane [10,11,15], which is the Si analogue of toluene, the $[M-2]^{+\bullet}$ and $[M-3]^+$ peaks are strong along with the $[M-1]^+$ peak, where M denotes the molecular mass. Recently, the dissociation of the phenylsilane molecular ion has been studied theoretically [11]. At low energies, the H_2 loss is favored, whereas the H• loss is favored as the energy increases. The silabenzylium ion is formed by the loss of H•, and the ion $[M-3]^+$ can be formed through the consecutive dissociations of the ions $[M-1]^+$ and $[M-2]^{+\bullet}$. For the dissociation of the aniline molecular ion, the loss of HNC occurs through ring opening and contraction and is more favored than the loss of H• [8]. In contrast, in the EI mass spectrum of phenylphosphine [13,15], which is the P analogue of aniline, the $[M-1]^+$, $[M-2]^{+\bullet}$, and $[M-3]^+$ peaks are strong, similar to phenylsilane. Recently, Letzel et al. [13] investigated the dissociation of the phenylphosphine molecular ion (**1a**) using tandem mass spectrometry and proposed reaction pathways for the loss H• and H_2 using density functional theory (DFT) calculations.

In this work, the theoretical potential energy surfaces (PESs) were examined for the main primary and secondary dissociations of **1a** (Scheme 1). Based on the PESs, Rice–Ramsperger–Kassel–Marcus (RRKM) [16] model calculations were carried out in order to obtain information on the detailed kinetics of the primary and secondary dissociations.

2. Computational methods

The molecular orbital calculations were performed with the Gaussian 03 suite of programs [17]. The geometry of the stationary points was optimized at the unrestricted B3LYP level of the DFT using the 6-31G(d) basis set. The transition state (TS) geometries that connected the stationary points were examined and checked by calculating the intrinsic reaction coordinates at the same level. For better accuracy of the energies, Gaussian-3 (G3) theory calculations using the B3LYP density functional method (G3//B3LYP) [18] were performed. In G3//B3LYP calculations, the geometries are obtained at the B3LYP/6-31G(d) level, and the zero point vibrational energies are obtained at the same level and scaled by 0.96.

Abbreviations: PES, potential energy surface; TS, transition state.

* Corresponding author. Tel.: +82 2 2260 8914; fax: +82 2 2268 8204.
E-mail address: jcchoe@dongguk.edu (J.C. Choe).

1387-3806/$ – see front matter © 2010 Elsevier B.V. All rights reserved.
doi:10.1016/j.ijms.2010.05.006

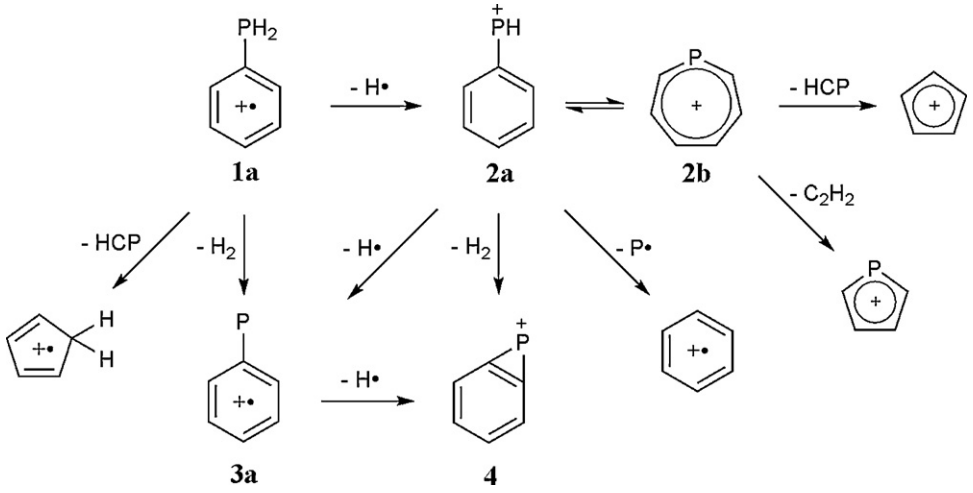

Scheme 1. Dissociation scheme of the phenylphosphine molecular ion **1a**.

All the other steps remain the same as the G3 method [19] with the exception of the values of the higher level correction parameters.

The RRKM expression was used to calculate the rate-energy dependence for individual unimolecular reaction steps that were involved in the selected reaction pathways [16]:

$$k(E) = \frac{\sigma N^{\ddagger}(E - E_0)}{h\rho(E)} \quad (1)$$

In this equation, E is the reactant internal energy, E_0 is the critical energy of the reaction, $N^{\ddagger}$ is the sum of the TS states, ρ is the density of the reactant states, σ is the reaction path degeneracy, and h is the Planck's constant. $N^{\ddagger}$ and ρ were evaluated through a direct count of the states using the Beyer–Swinehart algorithm [20].

3. Results and discussion

3.1. Primary dissociation

The following three reactions were the primary dissociations of **1a** that were investigated in this work.

$$C_6H_5PH_2^{+\bullet} \rightarrow C_6H_6P^+ + H^\bullet \quad (2)$$

$$C_6H_5PH_2^{+\bullet} \rightarrow C_6H_5P^{+\bullet} + H_2 \quad (3)$$

$$C_6H_5PH_2^{+} \rightarrow C_5H_6^{+\bullet} + HCP \quad (4)$$

The relative abundances of the $C_6H_6P^+$, $C_6H_5P^{+\bullet}$, and $C_5H_6^{+\bullet}$ peaks in the previously reported 70-eV EI mass spectrum were 22, 100, and 6%, respectively [15]. The optimized structure of **1a** showed that two H atoms of the phosphino group lay on the same side of the phenyl ring (Fig. 1). During the loss of H_2 (reaction (3)), first, the phosphino group rotated and then the two H atoms gradually moved away from P to form the phenylphosphinidene radical cation (**3a**). Similar 1,1-H_2 elimination was reported in the dissociation of the phenylsilane molecular ion [11]. Other types of H_2 elimination such as 1,2 elimination can compete with 1,1-H_2 elimination [21]. Since 1,3-H_2 elimination could compete with the 1,1-H_2 elimination in this case, we tried to locate the corresponding TS but failed. However, it is likely that the 1,3-H_2 elimination would not be important because its expected product (the benzophosphirene radical cation (**3b**) + H_2, which will be described in Section 3.2), lying 122 kJ mol^{-1} higher than **3a** + H_2, was less stable than the TS for the 1,1-H_2 elimination. Fig. 1 shows the potential energy diagram determined from the G3//B3LYP calculations. Formation of **3a** + H_2 was the most thermodynamically favorable channel in the primary dissociation of **1a** [22].

Two isomeric $C_6H_6P^+$ ions with planar six- and seven-membered ring structures were formed by the loss of H$^\bullet$ (reaction (2)). The phenylphosphenium ion (**2a**) was formed by a direct P—H bond cleavage. Its TS could not be located, indicating that the dissociation occurred via a loose TS without a reverse barrier, which was confirmed by scanning the PES. These products, **2a** + H$^\bullet$, were 140 kJ mol^{-1} less stable than **3a** + H_2. The 7-phospha-tropylium ion (**2b**), the seven-membered ring isomer of **2a**, was formed through three or four consecutive steps. The *exo*-7-phospha-norcaradiene radical cation (*exo*-**1b**) was formed as a result of the 1,2 shift of an H atom in the phosphino group. The 7-phospha-cycloheptatriene radical cation (**1c**) was formed by a ring expansion, and then **2b** was formed by a direct P—H bond cleavage. The *endo* rotamer of **1b** (*endo*-**1b**) was formed by the rotation of the PH group of *exo*-**1b** and also isomerized to **1c**.

Alternatively, *exo*-**1b** underwent isomerization to either **1d** or **1e** by a C···P bond cleavage with a 1,2-H shift. **1e** was formed by a rotation of the PH group of **1d** or directly from **1a** by a 1,3-H shift. The latter pathway (not shown in Fig. 1) was far less favored because of its high energy barrier, 211 kJ mol^{-1}. Alternatively, **1d** was formed from **1e** by consecutive 1,2-H shifts ("H-ring walk") via **1f**, **1g**, and **1h**, where **1h** was a rotamer of **1f**. Each of these five isophenylphosphine radical cations produced **2a** by elimination H$^\bullet$ from the CH_2 group. The TSs for the H$^\bullet$ elimination from **1f**, **1g**, and **1h** were not located, indicating the absence of reverse barriers. Both the TSs of **1d** and **1e** were 5 kJ mol^{-1} higher than the products, **2a** + H$^\bullet$. **1c** also underwent consecutive 1,2-H shifts to form **1i**, **1j**, and **1k**. The TSs for the formation of **2b** from **1i**, **1j**, and **1k** by elimination of H$^\bullet$ were 15, 20, and 13 kJ mol^{-1} higher than the products, **2b** + H$^\bullet$, respectively.

In the dissociation of the aniline molecular ion to form the cyclopentadiene radical cation, c-$C_5H_6^{+\bullet}$, HNC is the neutral product not HCN, even though HNC is much less stable than HCN [6,7]. However, in the dissociation of **1a**, HCP was the only partner of c-$C_5H_6^{+\bullet}$ because HPC was not a stable molecule. Several pathways were determined for the formation of c-$C_5H_6^{+\bullet}$ by loss of HCP. The pathway occurring via **1k** was the lowest energy pathway. The PES of this pathway is shown in Fig. 2. A five-membered ring intermediate, **1n**, was formed after the deformation of the seven-membered ring of **1k**. An ion–molecule complex, **1p**, was formed by a rotation of the HCP group and then dissociated to c-$C_5H_6^{+\bullet}$ and HCP. The highest barrier for the loss of HCP was energetically comparable to the formation of **2a**.

Considering only the energies that were from the PES, the loss of H_2 would be the most favored channel in the primary dissoci-

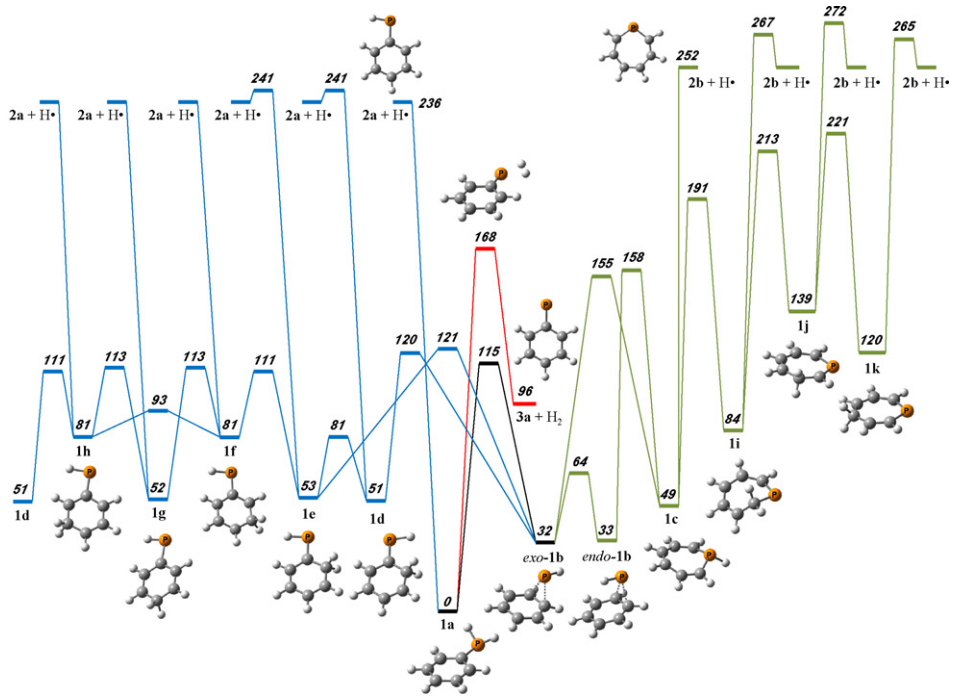

Fig. 1. Potential energy diagram for the loss of H_2 and H• from **1a**, which was derived from the G3//B3LYP calculations. The energies are presented in kJ mol^{-1}. The calculated total energy of **1a** was −573.5476900 hartrees.

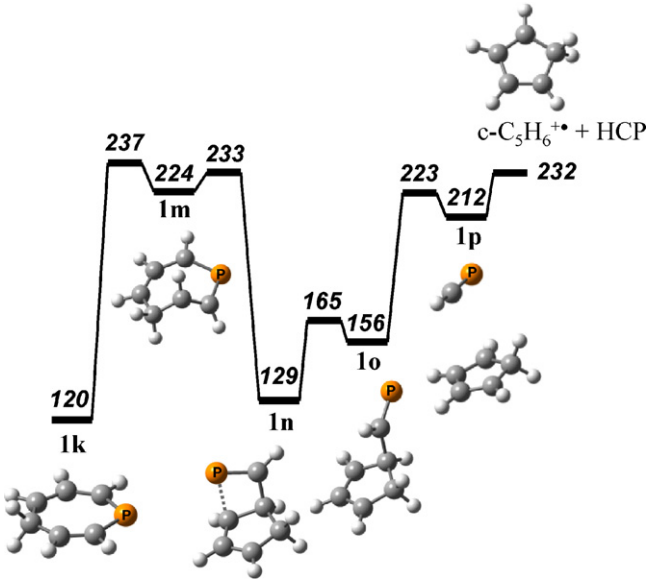

Fig. 2. Potential energy diagram for the lowest energy pathway of the loss of HCP from **1a**, occurring via **1m**. This diagram was derived from the B3LYP G3//B3LYP calculations. The energies are presented in kJ mol^{-1} and refer to **1a**.

ation, and the less favored channels, corresponding to the loss of H• and HCP, would compete with each other, resulting in similar yields. However, the PES shows that the rate of the loss H• is determined by a loose TS whereas that of the loss of HCP is determined by a tight TS. This suggests that the loss of H• would be kinetically favored over the loss of HCP. This prediction agrees with the small relative abundance of the $C_5H_6^{+\bullet}$ peak (6%) in the EI mass spectrum mentioned above. However, the kinetic effects of the loss of H_2 and H• could not be predicted without further calculation. The dissociation rate constants were calculated from the PES for the primary dissociation in order to investigate the competition between the loss of H_2 and H• with respect to the ion energy. For convenience, only the reaction pathways in Fig. 1 were included in this kinetic analysis. The other steps that were related to the loss of HCP were excluded because their contributions to the overall dissociation rate were small, and the main interest of this study was the competition between the loss of H_2 and H•.

First, the rate constants were calculated using the RRKM formalism of Eq. (1) for both the individual forward and reverse isomerizations between the stable species and the individual dissociation steps. The critical energies and vibrational frequencies obtained from the DFT calculations were used for the RRKM calculations. The vibrational frequencies were scaled down by a factor of 0.9614 suggested for the B3LYP/6-31G(d) calculation [23]. Uncertainties occurred in the RRKM calculations for the dissociation steps that did not have reverse barriers because their TSs were not located. These steps were **1a** → **2a** + H•, **1f** → **2a** + H•, **1g** → **2a** + H•, **1h** → **2a** + H•, and **1c** → **2b** + H•. The activation entropy ($\Delta S^{\ddagger}$), which defines the degree of looseness of the TS [16], was used in the calculations for these steps. The RRKM rate constants do not depend on the individual vibrational frequencies but on the $\Delta S^{\ddagger}$ [16,24]. According to the data compiled by Lifshitz and subsequent work [24], most of the $\Delta S^{\ddagger}$ values ranged from 13 to 46 J mol^{-1} K^{-1} (3.0–11 eu) at 1000 K for the reactions occurring via loose TSs. As an approximation, the frequencies for each loose TS were adjusted so that $\Delta S^{\ddagger}_{1000\,K}$ might be 7.0 eu, which was the middle value of the range. The $\Delta S^{\ddagger}_{1000\,K}$ values of 3.0 and 3.7 eu for the H• elimination from **1d** and **1i**, respectively, were calculated from the reactant and TS frequencies for comparison purposes. These TSs exhibited loose TS characteristics because the reverse barriers for these dissociation steps (5 and 15 kJ, respectively) were small. Considering these values, 7.0 eu is reasonable for $\Delta S^{\ddagger}_{1000\,K}$ in the dissociation steps without reverse barriers. The RRKM rate-energy dependence calculated for the important reaction steps is shown in Fig. 3. Second, the rate equations were set up for the reaction system including the isomerization and dissociation steps, and the MATLAB program was used to numerically solve the coupled differential equations [25–27]. The solution provided the time dependence of the con-

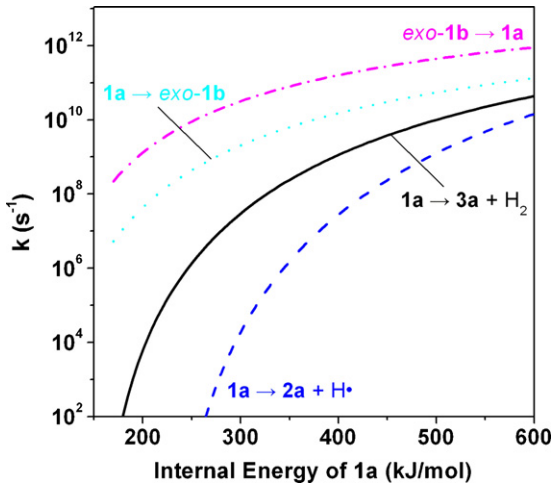

Fig. 3. RRKM rate-energy dependence for the selected reaction steps in the primary dissociation of **1a**.

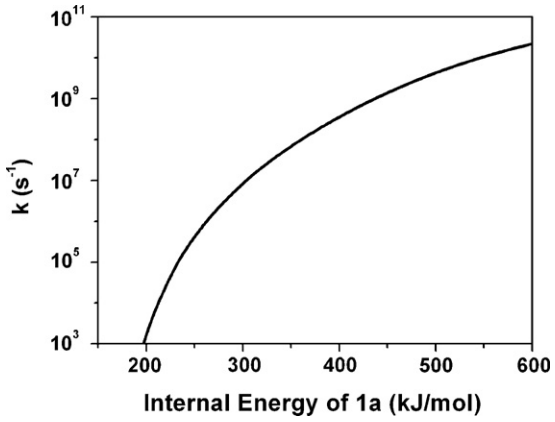

Fig. 4. Theoretical rate-energy dependence for the primary dissociation of **1a**. The contribution from the loss of HCP was ignored for convenience.

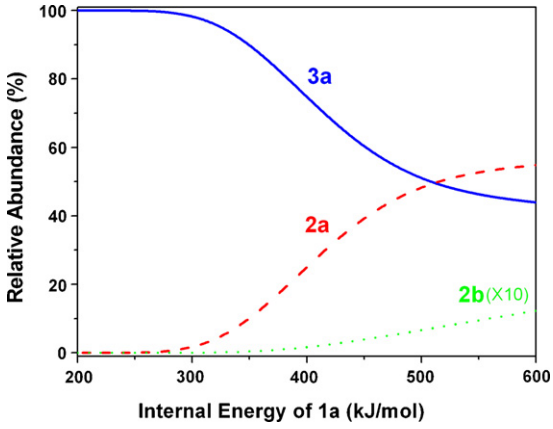

Fig. 5. Theoretical relative abundances of the products that were formed in the primary dissociation of **1a**. The **2a** value is multiplied by a factor of 10. The contribution from the loss of HCP was ignored for convenience.

centrations of **1a**, the intermediates, and the product ions at a specific ion internal energy. Finally, the overall dissociation rate constant was obtained by fitting an exponential law to the sum of time dependence of the concentrations of **1a** and all the intermediates. This procedure was repeated for a range of the internal energy values.

Fig. 4 shows the overall dissociation rate-energy dependence. The relative abundances of the product ions, **2a**, **2b**, and **3a**, were also obtained from the time dependence of their concentrations as a function of the internal energy (Fig. 5). Letzel et al. [13] presented the metastable ion spectrum of **1a**, which only contained one signal that was caused by the H_2 loss. In a usual metastable ion spectrum, only the dissociations that occur on the microsecond time scale ($k = 10^5$–$10^6\ s^{-1}$) are detected. The rate-energy dependence in Fig. 4 predicted that the internal energies of the molecular ions **1a** that underwent the metastable dissociation were in the range of 230–260 kJ mol^{-1}. At these energies, the H_2 loss was the only dissociation channel, as shown in Fig. 5, which agreed well with the metastable ion experimental results. Letzel et al. [13] demonstrated that H scrambling occurred before the loss of H• using the metastable ion experiment for the $C_6H_5PD_2^{+\bullet}$ ion. They pointed out that a fast positional exchange of H and D atoms was possible before the dissociation because of the degenerate isomerization of **1b** ⇌ **1b** by a PH ring walk. In this study, the critical energies for the PH ring walk of *exo*- and *endo*-**1b** were 24 and 13 kJ mol^{-1}, respectively, indicating that the process was very fast. The PH ring walk can contribute to the H scrambling at low energies because the calculated rate for **1a** → *exo*-**1b** was much faster than the dissociation steps below 300 kJ mol^{-1} (Fig. 3). The subsequent isomerization barriers to and between the isophenylphosphine radical cations were comparable to the barrier for **1a** → *exo*-**1b** (Fig. 1), indicating that these isomerizations can also contribute to the H scrambling. However, the isomerizations to the seven-membered ring isomers would hardly contribute to the H scrambling because of their high barriers.

Fig. 5 predicts that the H• loss gradually becomes important as the energy increases, and its product ion, $C_6H_6P^+$, mainly has the structure of **2a**. The $C_6H_6P^+$ peak was absent in the metastable ion spectrum but appeared in the EI mass spectrum because the molecular ions that were generated by 70-eV EI had a broad internal energy distribution up to nearly 10 eV. In Fig. 5, the competition between the formation of **2a** and **3a** was typical because **2a** was formed by a direct bond cleavage without a reverse barrier and **3a** was formed through a rearrangement.

As mentioned above, **2a** was predicted as the main product in the loss of H•. The [**2a**]/[**2b**] ratio was estimated to be 73 at 500 kJ mol^{-1}. Some factors affected their relative abundances. The first factor was the energy. Generally, the more stable product is favored when other conditions are similar. **2a** was 16 kJ mol^{-1} lower than **2b**. The second factor was the number of reaction pathways that led to each product. Assuming that the isomerizations to the intermediates rapidly occurred before the dissociations, the number of effective reaction pathways depended on the reaction path degeneracy (σ in Eq. (1)) corresponding to each dissociation step. **2a** was formed directly from **1a** and via **1d**, **1e**, **1f**, **1g**, and **1h**, through six dissociation steps, with $\sigma = 2$ for all of the steps. The formation of **2b** occurred through four different steps via **1c**, **1i**, **1j**, and **1k**, with a value of $\sigma = 1$ and $\sigma = 2$ for the first step and the latter three steps, respectively. Therefore, the formation of **2a** was more favorable. Moreover, the isomerization barriers for the seven-membered ring intermediates were higher than those for the isophenylphosphine ions, making the formation of **2a** more favorable. The third factor was the looseness of the TSs of the dissociation steps. As mentioned above, the RRKM rate constants depend on the $\Delta S^{\ddagger}$. A value of 7.0 eu was used for $\Delta S^{\ddagger}_{1000\,K}$ in the RRKM calculations for the H• elimination steps from **1a**, **1f**, **1g**, **1h**, and **1c**. Even when assuming that the dissociation step, **1c** → **2b** + H•, occurred via an extremely loose TS that was characterized by $\Delta S^{\ddagger}_{1000\,K} = 11$ eu, the theoretical [**2a**]/[**2b**] ratio was still large, 14 at 500 kJ mol^{-1}.

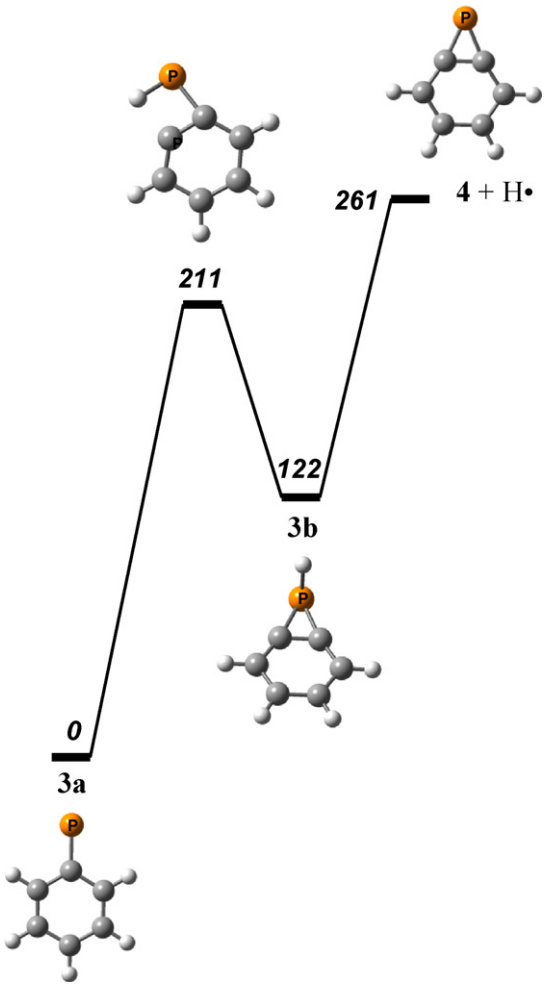

Fig. 6. Potential energy diagram for the loss of H• from **3a,** which was derived from the G3//B3LYP calculations. The energies are presented in kJ mol^{-1}. The calculated total energy of **3a** was −572.3436661 hartrees.

3.2. Secondary dissociation

The further dissociations of the two major product ions of the primary dissociation of **1a** were investigated.

$$C_6H_5P^{+\bullet} \rightarrow C_6H_4P^+ + H^\bullet \quad (5)$$

$$C_6H_6P^+ \rightarrow C_6H_5P^{+\bullet} + H^\bullet \quad (6)$$

$$C_6H_6P^+ \rightarrow C_6H_4P^+ + H_2 \quad (7)$$

$$C_6H_6P^+ \rightarrow C_4H_4P^+ + C_2H_2 \quad (8)$$

$$C_6H_6P^+ \rightarrow C_5H_5^+ + HCP \quad (9)$$

$$C_6H_6P^+ \rightarrow C_6H_6^{+\bullet} + P^\bullet \quad (10)$$

The relative abundances of the $C_4H_4P^+$, $C_6H_6^{+\bullet}$, and $C_5H_5^+$ peaks were 12, 9, and 9%, respectively, in the previously reported 70-eV EI mass spectrum [15]. According to the report by Letzel et al. [13], reaction (5) was the only dissociation of the metastable $C_6H_5P^{+\bullet}$ ion. This reaction occurred through two consecutive steps (Fig. 6). As the P atom of **3a** approached the ortho position, the ortho-H shifted to the P atom to form the benzophosphirene radical cation (**3b**). Then the benzophosphirenium cation (**4**) was formed by the direct P—H bond cleavage of **3b**. Alternatively, **4** was also formed from **2a** (reaction (7)) by 1,2-H_2 elimination through two similar consecutive steps. As the P atom approached the *cis*-ortho position, the *cis*-ortho-H shifted to the P atom to form an ion–molecule complex, **2c** (Fig. 7). The subsequent dissociation step to **4** + H_2 occurred without a reverse barrier. Comparing the overall energy barriers, **1a** → **3a** (+ H_2) → **4** + H• was energetically favored over **1a** → **2a** (+ H•) → **4** + H_2 by a value of 162 kJ mol^{-1} and hence was the main pathway in the formation of **4**.

2a also underwent other dissociations. By a direct P—H bond cleavage, **2a** dissociated to **3a** + H• (reaction (6)). However, this was not the lowest energy pathway for the formation of **3a** from **1a** because the overall energy of **1a** → **2a** (+ H•) → **3a** + H• was 530 kJ mol^{-1}, which was much higher than the energy barrier (168 kJ mol^{-1}) for **1a** → **3a** + H_2. Several different pathways were found for reactions (8) and (9), but only the lowest energy pathways will be described here. First, **2a** isomerized to **2b**. As the P atom of **2a** approached the *trans*-ortho position, the H atom of the PH group shifted to the ipso position, and the P atom migrated to the ortho position to form a P substituted benzenium ion, **2d** (Fig. 7). **2d** easily isomerized to a more stable 7-phospa-norbornadienyl cation (**2e**). Alternatively, after the P atom of **2d** moved back to the original ipso position, it was inserted into the ring to form **2b**. Then **2b** could either lose C_2H_2 or HCP. A bicyclic isomer, **2g**, was formed from the distorted seven-membered ring intermediate, **2f**. After the four-membered ring opened, the planar five-membered ring cation, c-$C_4H_4P^+$, was formed by the elimination of acethylene, C_2H_2. Another distorted seven-membered ring intermediate, **2i**, that was formed from **2b** isomerized to a five-membered ring intermediate, **2j**, and subsequently eliminated HCP to form the cyclopentadienylium ion, c-$C_5H_5^+$.

As shown in Fig. 7, the isomerization barrier between **2a** and **2b** was lower than the dissociation barriers for **3a** and **4**, suggesting that the isomerization rapidly occurred before the dissociations. The RRKM calculations were carried out for the four reactions, **2a** → **3a** + H•, **2a** → **4** + H_2, **2a** → **2b**, and **2b** → **2a**, in order to compare their rates. For the first reaction, 7.0 eu was used for $\Delta S^{\ddagger}_{1000\,K}$, as above. The forward isomerization step of the second reaction, **2a** → **2c**, was the rate limiting step because the dissociation step, **2c** → **4** + H_2, was very fast. Therefore, the rate for **2a** → **2c** was approximately the same as the second reaction. The forward and reverse isomerizations between **2a** and **2b** were assumed to occur through one TS that connected **2a** and **2d** because the passage was the rate-limiting step in each direction. The rate-energy dependence is shown in Fig. 8. At low energies, the interconversion between **2a** and **2b** rapidly occurred before the dissociations, and the H_2 loss was favored over the H• loss. As the energy increased, the H• loss became more favored and competed with the interconversion.

The peaks corresponding to the loss of H•, H_2, C_2H_2, and HCP appeared along with a weak $C_6H_6^{+\bullet}$ peak in the previously reported metastable ion spectrum of $C_6H_6P^+$ that was generated from ionized phenylphosphine [13]. In Fig. 7, the required energies were similar for reactions (6)–(9), which corresponded to the major peaks that were detected, in accordance with this experiment. **2e** lost a P atom to form the benzene radical cation. An intersystem-crossing must occur from the singlet hypersurface in order to produce a P atom in a quartet state ($^4P^\bullet$), which was more stable than $^2P^\bullet$ (Fig. 7). The crossing point calculations were not performed because they were beyond the scope of this work.

Muedas et al. reported collision-induced dissociation (CID) spectra of the $C_6H_6P^+$ ions prepared by two different techniques [14]. They suggested that the precursor ions generated by ion–molecule reaction had mainly the structure of **2b**, and those generated from phenylphosphine had mainly the structure of **2a**. The two CID spectra are similar in that the detected fragment ions are almost the same but different in their relative abundances. For example, the $C_6H_5^+$ peak was more abundant in the CID of the $C_6H_6P^+$ ions having mainly **2a** structure. Accepting their suggestion for the assignment of the precursor ions, the similarity of the two CID patterns can be

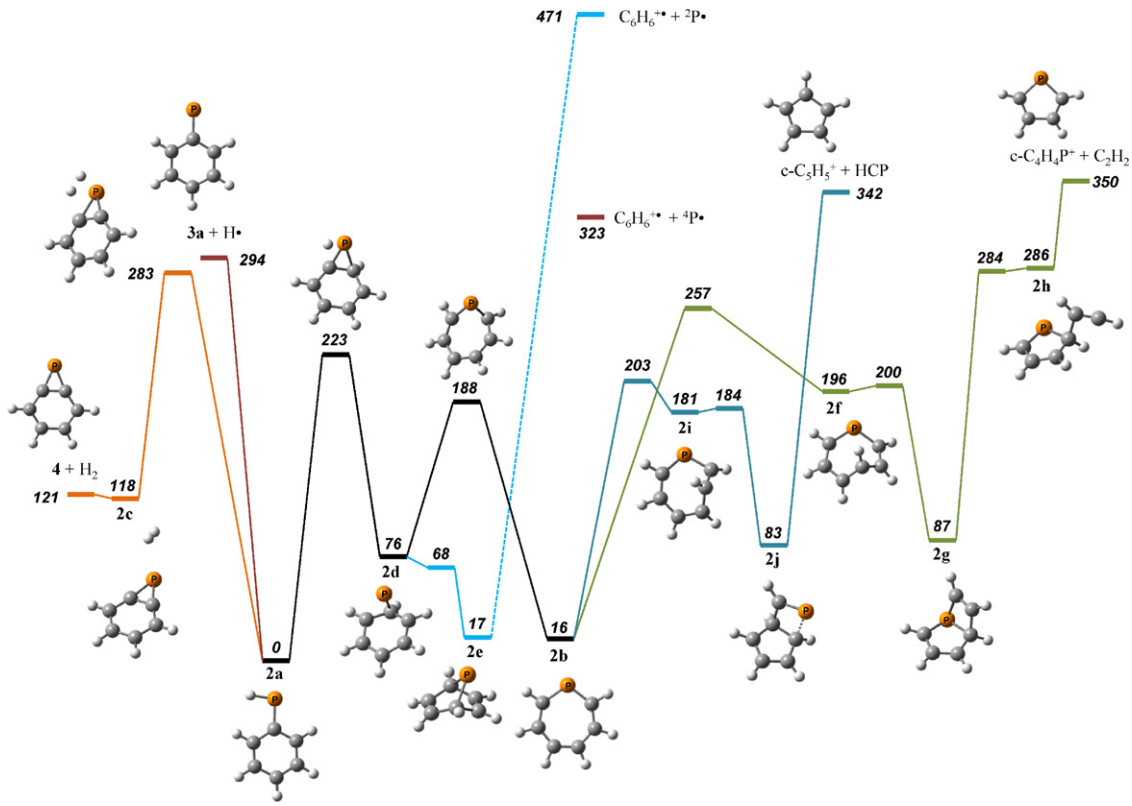

Fig. 7. Potential energy diagram for the dissociation of **2a,** which was derived from the G3//B3LYP calculations. The energies are presented in kJ mol^{-1}. The calculated total energy of **2a** was −572.9568138 hartrees.

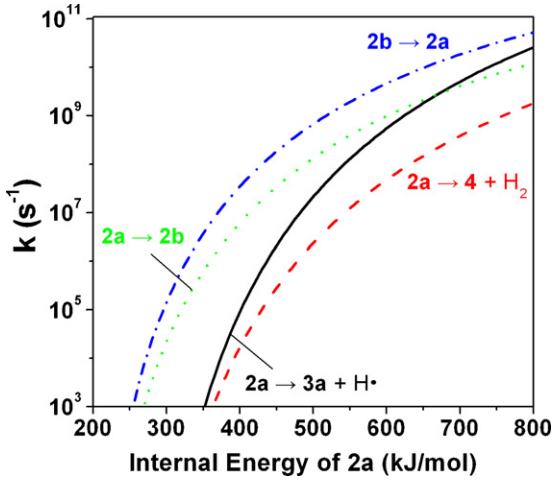

Fig. 8. RRKM rate-energy dependence for the selected reaction channels in the dissociation of **2a**.

explained by the fast interconversion between **2a** and **2b** occurring at low energies and the difference can be explained by the occurrence of dissociations without the interconversion at high energies. This is possible because the precursor ions undergoing CID generally possess internal energy of a broad distribution.

4. Conclusions

The kinetic analysis showed that the formation of **3a** by the loss of H_2 was the only dissociation channel at low internal energies of **1a**. However, at high energies, the formation of **2a** by the loss of H• competed with the loss of H_2. Before the dissociation at low energies, the isomerization of **1a** to several isophenylphosphine radical cations occurred rapidly and was subsequently followed by the elimination of H• to form **2a**. The consecutive reactions of **1a** → **3a** (+ H_2) → **4** + H• were the main pathway for the formation of **4**. The energy barriers were similar for the formation of **3a** + H•, **4** + H_2, c-$C_4H_4P^+$ + C_2H_2, and c-$C_5H_5^+$ + HCP from **2a**. Various rearrangement mechanisms including ring expansion, contraction, closure, and opening were involved in the investigated dissociations. The reported EI and metastable ion mass spectra were well explained by the present results.

The formation of c-$C_5H_6^+$ by the loss of HCP was not important to the dissociation of **1a**, whereas the loss of HNC was the predominant dissociation channel of the aniline molecular ion, which is the N analogue of **1a**. The main dissociations of **1a** were caused by the loss of H_2 and H•. The remarkable difference between the dissociation patterns of **1a** and the aniline ion was probably observed because the P—H bond was more labile than the N—H bond. The loss of H_2 and H• from the aniline ion are suppressed due to their high energy requirement relative to the loss of HNC. The formation of the benzene radical cation from **1a** by consecutive loss of H• and P•, not observed in the dissociation of the aniline ion, reflects the fact that the C—P bond is weaker than the C—N bond.

Acknowledgments

This work was supported by the Korea Research Foundation Grant funded by the Korean Government (KRF-2008-313-C00403). The authors would like to thank Ji Hye Kim for her assistance in use of the MATLAB program. SYK acknowledges the award of a Park Kwan Ho Scholarship from Dongguk University.

References

[1] F.S. Huang, R.C. Dunbar, Int. J. Mass Spectrom. Ion Process. 109 (1991) 151.
[2] C. Lifshitz, Acc. Chem. Res. 27 (1994) 138.

[3] H.F. Grützmacher, N. Harting, Eur. J. Mass Spectrom. 9 (2003) 327.
[4] J.C. Choe, J. Phys. Chem. A 110 (2006) 7655.
[5] T. Baer, T.E. Carney, J. Chem. Phys. 76 (1982) 1304.
[6] C. Lifshitz, P. Gotchiguian, R. Roller, Chem. Phys. Lett. 95 (1983) 106.
[7] M.T. Nguyen, in: Z. Rappoport (Ed.), The Chemistry of Anilines, Wiley, New York, 2007.
[8] J.C. Choe, N.R. Cheong, S.M. Park, Int. J. Mass Spectrom. 279 (2009) 25.
[9] R.L. Jarek, S.K. Shin, J. Am. Chem. Soc. 119 (1997) 6376.
[10] J.C. Choe, Rapid Commun. Mass Spectrom. 17 (2003) 207.
[11] J.C. Choe, Int. J. Mass Spectrom. 237 (2004) 1.
[12] P.C. Nam, M.T. Nguyen, A.K. Chandra, J. Phys. Chem. A 108 (2004) 11362.
[13] M. Letzel, H.F. Grützmacher, D. Stein, H. Grützmacher, Dalton Trans. (2008) 3282.
[14] C.A. Muedas, D. Schroeder, D. Suelzle, H. Schwarz, J. Am. Chem. Soc. 114 (1992) 7582.
[15] NIST Mass Spec Data Center, S.E. Stein, director, "Mass Spectra" in NIST Chemistry WebBook, NIST Standard Reference Database Number 69, P.J. Linstrom, W.G. Mallard (Eds.), National Institute of Standards and Technology, Gaithersburg MD, 20899, http://webbook.nist.gov, (retrieved May 17, 2010).
[16] T. Baer, W.L. Hase, Unimolecular Reaction Dynamics: Theory and Experiments, Oxford University Press, New York, 1996.
[17] M.J. Frisch, G.W. Trucks, H.B. Schlegel, G.E. Scuseria, M.A. Robb, J.R. Cheeseman, J.A. Montgomery Jr., T. Vreven, K.N. Kudin, J.C. Burant, J.M. Millam, S.S. Iyengar, J. Tomasi, V. Barone, B. Mennucci, M. Cossi, G. Scalmani, N. Rega, G.A. Petersson, H. Nakatsuji, M. Hada, M. Ehara, K. Toyota, R. Fukuda, J. Hasegawa, M. Ishida, T. Nakajima, Y. Honda, O. Kitao, H. Nakai, M. Klene, X. Li, J.E. Knox, H.P. Hratchian, J.B. Cross, V. Bakken, C. Adamo, J. Jaramillo, R. Gomperts, R.E. Stratmann, O. Yazyev, A.J. Austin, R. Cammi, C. Pomelli, J.W. Ochterski, P.Y. Ayala, K. Morokuma, G.A. Voth, P. Salvador, J.J. Dannenberg, V.G. Zakrzewski, S. Dapprich, A.D. Daniels, M.C. Strain, O. Farkas, D.K. Malick, A.D. Rabuck, K. Raghavachari, J.B. Foresman, J.V. Ortiz, Q. Cui, A.G. Baboul, S. Clifford, J. Cioslowski, B.B. Stefanov, G. Liu, A. Liashenko, P. Piskorz, I. Komaromi, R.L. Martin, D.J. Fox, T. Keith, M.A. Al-Laham, C.Y. Peng, A. Nanayakkara, M. Challacombe, P.M.W. Gill, B. Johnson, W. Chen, M.W. Wong, C. Gonzalez, J.A. Pople, Gaussian 03, Revision C.02, Gaussian, Inc., Wallingford, CT, 2004.
[18] A.G. Baboul, L.A. Curtiss, P.C. Redfern, J. Chem. Phys. 110 (1999) 7650.
[19] L.A. Curtiss, K. Raghavachari, P.C. Redfern, V. Rassolov, J.A. Pople, J. Chem. Phys. 109 (1998) 7764.
[20] T. Beyer, D.R. Swinehart, ACM Commun. (1973) 379.
[21] E. Uggerud, Mass Spectrom. Rev. 18 (1999) 285.
[22] We found that the energy of **3a** calculated by DFT overestimated significantly compared to the G3 calculation. According to the BHLYP/6-311 + G(2d,p)//BHLYP/6-31 + G(d) calculations by Letzel et al., the sum of the enthalpies of formation at 298 K of **3a** and H_2 is 243 kJ mol^{-1} relative to **1a**, much higher than their sum of the present G3//B3LYP energies, 96 kJ mol^{-1}. We performed the B3LYP/6-311 + G(3df,2p)//B3LYP/6-31G(d) and CBS-QB3 calculations for comparison purposes. The B3LYP energies of **3a** + H_2 and the TS were 189 and 170 kJ mol^{-1}, respectively, and an ion–molecule complex was found between them as an intermediate. The CBS-QB3 energies of **3a** + H_2 and the TS were 100 and 172 kJ mol^{-1}, respectively. The CBS result agreed with the G3 result, while the DFT result overestimated the energy of **3a** significantly.
[23] A.P. Scott, L. Radom, J. Phys. Chem. A 100 (1996) 16502.
[24] C. Lifshitz, Adv. Mass Spectrom. 11 (1989) 713.
[25] J.I. Steinfeld, J.S. Francisco, W.L. Hase, Chemical Kinetics and Dynamics, Prentice Hall, Englewood Cliffs, 1989.
[26] J. Seo, H.-I. Seo, S.-J. Kim, S.K. Shin, J. Phys. Chem. A 112 (2008) 6877.
[27] S. Schulze, A. Paul, K.-M. Weitzel, Int. J. Mass Spectrom. 252 (2006) 189.